Journal of Applied Physics ARTICLE pubs.aip.org/aip/jap

Experimental determination of intrinsic carrier density in 4H-SiC based on electron diffusion current in an npn bipolar junction transistor

Cite as: J. Appl. Phys. **134**, 234502 (2023); doi: 10.1063/5.0180737
Submitted: 11 October 2023 · Accepted: 26 November 2023 ·
Published Online: 15 December 2023

Satoshi Asada,[1,a)] Koichi Murata,[1] Hajime Tanaka,[2] and Hidekazu Tsuchida[1]

AFFILIATIONS

[1]Central Research Institute of Electric Power Industry (CRIEPI), 2-6-1 Nagasaka, Yokosuka, Kanagawa 240-0196, Japan
[2]Division of Electrical, Electronic and Infocommunications Engineering, Osaka University, Suita, Osaka 565-0871, Japan

[a)]**Author to whom correspondence should be addressed:** asada3760@criepi.denken.or.jp

ABSTRACT

The intrinsic carrier density of 4H-SiC at temperatures ranging from 294 to 595 K was derived by analyzing a collector current in an npn-type SiC bipolar junction transistor, the structure of which was designed based on a device simulation. The obtained intrinsic carrier density was in good agreement with the value calculated from the bandgap and effective densities of states taking multiple and non-parabolic SiC bands into account. The coincidence of the intrinsic carrier density obtained by these two different approaches indicates the usefulness of the proposed method and the validity of the evaluated value of intrinsic carrier density. The temperature dependence of the bandgap was also estimated from the deduced intrinsic carrier density and compared with an empirical formula. The derived bandgap agreed well with the empirical formula showing bandgap shrinkage at high temperatures. The errors in evaluating the intrinsic carrier density and the bandgap caused by the estimation of the hole density and electron mobility in the base layer are also discussed for the proposed method.

I. INTRODUCTION

An intrinsic carrier density is a fundamental physical property of semiconductor materials, which significantly impacts a carrier recombination and injection in semiconductor devices because the intrinsic carrier density determines the thermal equilibrium condition. Insights into the intrinsic carrier density are crucial for analyzing the electrical characteristics of devices and designing the device structures. However, the intrinsic carrier density is extremely small at room temperature in general and far lower than a carrier density generated from doped impurities in the semiconductor material. This makes it difficult to determine the value from the electrical characteristics of the material.

Accordingly, the intrinsic carrier density is generally estimated from the bandgap and effective densities of states (effective mass) for electrons and holes,[1,2] which are experimentally obtained by optical absorption and cyclotron resonance measurement, respectively.[3–7] However, these experiments are usually performed at low temperatures: the former experiment is performed at a temperature ranging from 4.2 to 300 K and the latter one is conducted at below 10 K according to the references. Hence, the quantitative validity of the intrinsic carrier density deduced from the measured bandgap and effective mass contains uncertainness at elevated temperatures. It is worth developing alternative methods, including electrical measurements, to improve the validity of the value of intrinsic carrier density.

In the case of silicon (Si), as a determination method of the intrinsic carrier density from electrical characteristics, the conductivity of silicon was measured at elevated temperatures, and the intrinsic carrier densities at high temperatures were deduced. Using these values, extrapolative values at lower temperatures were then estimated.[8] This experimental approach effectively provided the intrinsic carrier density of silicon over a wide temperature range, which was in good agreement with the calculated value and provided reliable results.

However, the measurement method used for Si cannot be applied to wide bandgap (>3 eV) semiconductor materials because the intrinsic carrier density is too small to be measurable at high temperatures, exceeding the limitation of the measurement

equipment (>1000 K). In fact, for example, the intrinsic carrier density of 4H-silicon carbide (SiC), with a bandgap of around 3.26 eV at room temperature, was solely determined based on the bandgap and effective densities of states.[2] The validity of values was not confirmed from electrical measurements, despite numerous studies to date on SiC as an attractive semiconductor material, with scope to reduce the energy loss of power electronics systems considerably.[9–13] Currently, the intrinsic carrier density of wide bandgap materials cannot be obtained from electrical characteristics, and a universal solution should be devised.

To evaluate the intrinsic carrier density from the electrical characteristics, there will inevitably be a need to fabricate devices and measure the current–voltage (I–V) characteristics. Among various semiconductor devices, a bipolar junction transistor (BJT) is suitable for the present purpose, because a collector current in the BJTs with a uniform base doping concentration uniquely comprises a diffusion current due to the minority carrier in the base layer.[14] This eliminates the need to segregate the electron, hole, diffusion, and recombination currents when analyzing the electrical characteristics, which is a clear advantage of adopting the BJTs.

Numerous previous investigations have significantly refined the technique and knowledge for SiC device fabrication and already spawned many excellent SiC devices, including BJTs.[15–22] Achieving further advanced SiC devices will depend on stricter design based on an accurate device simulation, where the exact intrinsic carrier density is essential. Accordingly, in this study, we demonstrate an experimental method to determine the intrinsic carrier density of SiC by fabricating a SiC BJT and evaluating the collector current.

II. HOW TO DETERMINE INTRINSIC CARRIER DENSITY

Figure 1 schematically illustrates a basic npn-type BJT with a uniform base doping concentration to explain how the intrinsic carrier density is estimated. The collector current in the npn-type BJT is determined by the electron diffusion in the base layer and expressed as

$$J_C = eD_n \frac{dn}{dx}. \tag{1}$$

Here, J_C, e, D_n, and n denote the collector current density, elementary charge, diffusion coefficient of the electron, and electron density, respectively. The direction x is indicated in Fig. 1 by the black arrow from the emitter to the collector layer.

When the diffusion length of the electron in the base layer is longer than the base width of the BJT, the electron density distribution in the base layer becomes almost linear, as depicted by the red line in the upper side of Fig. 1,[14] and the collector current is approximately expressed as

$$J_C \approx eD_n \frac{n_{EB}}{W_B}. \tag{2}$$

Here, n_{EB} and W_B denote the injected electron density at the emitter/base junction and base width. The injected electron density is determined by the hole density p_B in the base layer, intrinsic carrier density n_i, and applied voltage V_{BE} on the emitter/base junction, based on which Eq. (2) transforms to

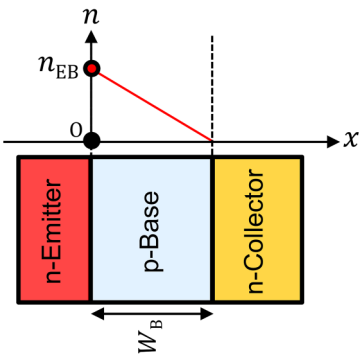

FIG. 1. Schematic illustration of a basic npn-type BJT with a uniform base doping concentration. The red line on the upper side of the device structure denotes the electron density distribution in the base layer when the diffusion length of electrons in the base layer is longer than the base width.

$$J_C \approx kT\mu_n \frac{n_i^2}{W_B p_B} \exp\left(\frac{eV_{BE}}{kT}\right). \tag{3}$$

Here, k and T denote the Boltzmann constant and temperature, respectively, and the diffusion coefficient of electron is transformed using the electron mobility μ_n according to Einstein equation $D_n = \mu_n kT/e$. This allows the intrinsic carrier density to be deduced from the pre-exponential factor of the collector current density, which is obtained by measuring the dependence of the collector current density on the applied base voltage.

III. EXPERIMENT

Figure 2(a) exhibits the schematic structure of a fabricated mesa-structure npn-type SiC BJT, the thickness and doping concentration of which are indicated individually in the figure. Here, the microscopic image of the fabricated BJT is also presented on the right side of the illustration. The doping concentration and the base layer thickness, which are the important parameters in the present study, were obtained by performing the secondary ion mass spectrometry (SIMS) measurement and examining the nitrogen and aluminum (Al) concentration from the top of the emitter layer to a depth of 8 μm. Figure 2(b) indicates the result of the SIMS measurement. In the base layer, although the aluminum concentration is slightly graded, the gradient is so small that the impacts of the gradation on the electrical characteristics are ignorable, which is confirmed by a device simulation (not shown). The base doping concentration can be regarded as uniform and the average concentration of 7.8×10^{16} cm^{-3} is adopted for the analyses.

Although a base layer in SiC BJTs is generally designed with a very thin thickness of less than 500 nm to achieve a high current gain,[23–28] we fabricated the BJT with a thick base layer (3.7 μm) to avoid an impact of the depletion region of the emitter/base and base/collector junctions, which effectively decreases the base width and causes an estimation error of the intrinsic carrier density. Figure 2(c) shows the electron density distribution in the base layer of the fabricated BJT when the base voltage of 2.5 V is applied with

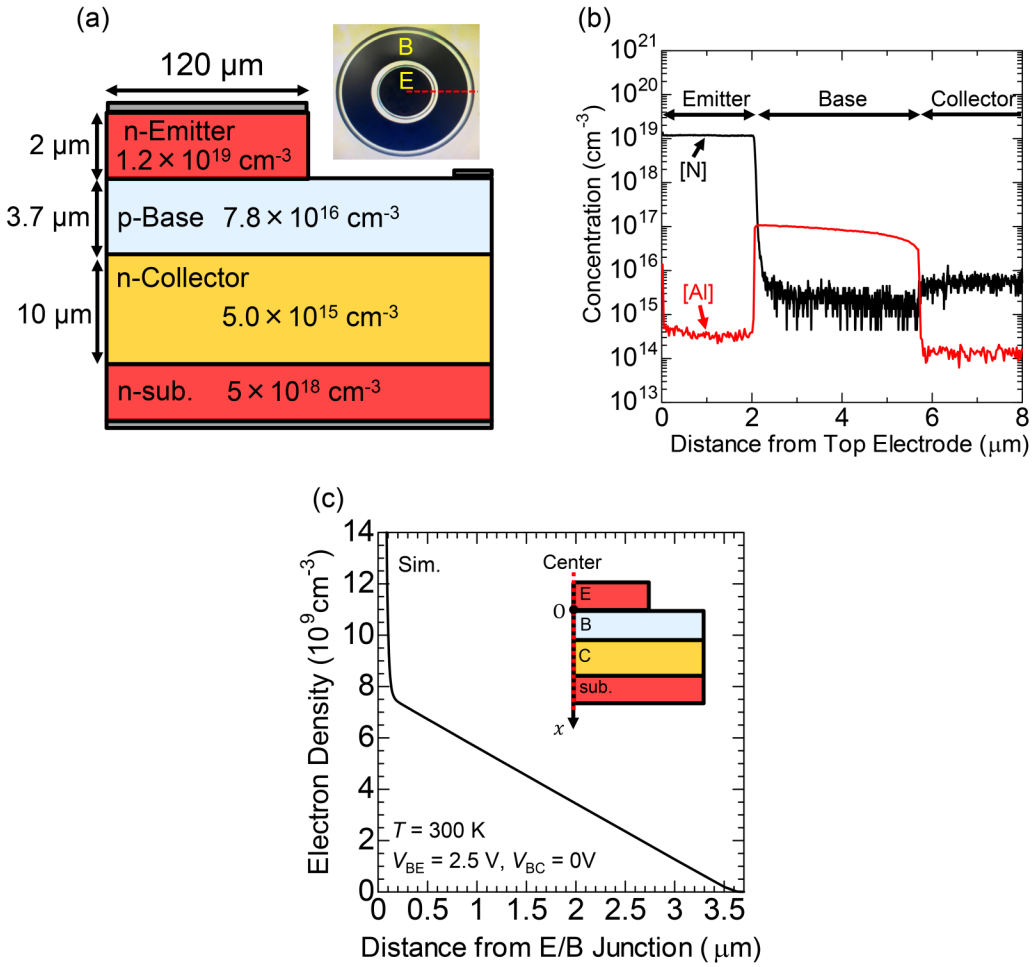

FIG. 2. (a) A schematic illustration of the fabricated BJT at the cross section indicated by the red dashed line in the microscopic image, presented on the right of the illustration. The yellow letters E and B in the microscopic image denote the emitter and base contacts, respectively. (b) The SIMS profile of the SiC epilayer utilized for the fabrication of the BJT. (c) The simulated electron density distribution at the temperature of 300 K in the base layer with the applied base voltage of 2.5 V. The distribution was obtained at the cross section of the center of the emitter finger, indicated by the red dashed line in the inset.

retaining the base–collector voltage to zero. It is simulated by utilizing Silvaco TCAD-Atlas device, assuming a carrier lifetime in the base layer of 100 ns.[28–31] In this assumption, the electron diffusion length becomes 8–15 μm at a temperature of 300–600 K, which is longer than the base width. Accordingly, the electron density is distributed linearly in the base layer and the collector current could be approximately expressed by Eq. (3) in the temperature range.

The emitter finger size of power SiC BJTs is usually designed to be around 10 μm to mitigate the current crowding effect due to the base spreading resistance.[32–36] Here, the current crowding effect indicates a localized collector current density at the edge side of the emitter finger. This is because the applied voltage on the emitter/base junction declines gradually at the center side due to the base spreading resistance. However, a large emitter finger size of 120 μm was employed in the present study because a low voltage region is analyzed to obtain the pre-exponential factor of the collector current and the voltage drop in the base layer due to the base spreading resistance is ignorable. Having a large emitter finger minimizes errors related to both the active area misestimation and edge effects, such as electric field accumulation at the emitter mesa sidewall.

The dependence of collector current on the applied base voltage of the fabricated BJT was measured at temperatures from 294 to 595 K. Precise temperature monitoring is essential for accurate analysis. Accordingly, both the fabricated SiC BJT and a 5 mm square SiC chip—outfitted with a thermocouple for temperature measurement—were placed on the same heated aluminum nitride substrate during the electrical characterization of the SiC BJT.

IV. RESULTS AND DISCUSSION

Figure 3(a) shows the collector current density as a function of the applied base voltage at various temperatures from 294 to 595 K.

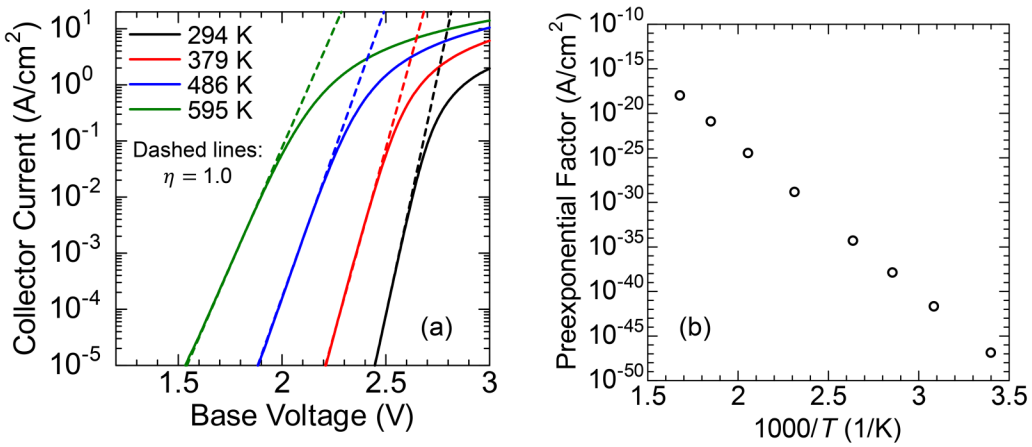

FIG. 3. (a) The dependence of the collector current density on the applied base voltage at various temperatures ranging from 294 to 595 K. The base–collector voltage was retained to be zero during the base voltage sweep. The dashed lines indicate the calculated current–voltage characteristics for each temperature assuming the ideality factor η of unity. (b) Temperature dependence of the pre-exponential factors of the measured collector currents.

Here, three BJTs were fabricated and measured on the same wafer, the electrical characteristics of which were confirmed to be identical. The dashed lines in the figure are the calculated I–V characteristics for each temperature assuming an ideality factor of unity ($\eta = 1.0$). As seen, the ideality factor of the measured collector current at the low current region becomes unity at each temperature, proving that the measured collector current purely comprises the diffusion current and is expressed by Eq. (3). Figure 3(b) plots the temperature dependent pre-exponential factors of the measured collector currents, which were obtained by fitting the calculated I–V characteristics ($\eta = 1.0$) to the experimental ones. Extracting the pre-exponential factors allows the intrinsic carrier density to be obtained.

To obtain the intrinsic carrier density from Eq. (3), the hole density p_B and electron mobility μ_n in the base layer must be determined. In the present study, the hole density in the base layer was estimated based on the semiconductor statistics assuming a single Al acceptor level, the ionization energy ΔE_{Al} of which ranges from 190 to 220 meV according to previous studies.[37–41] Figure 4(a) shows the temperature dependence of the calculated hole density in the base layer, the value of which peaks and reaches a minimum with ionization energy of 190 and 220 meV,

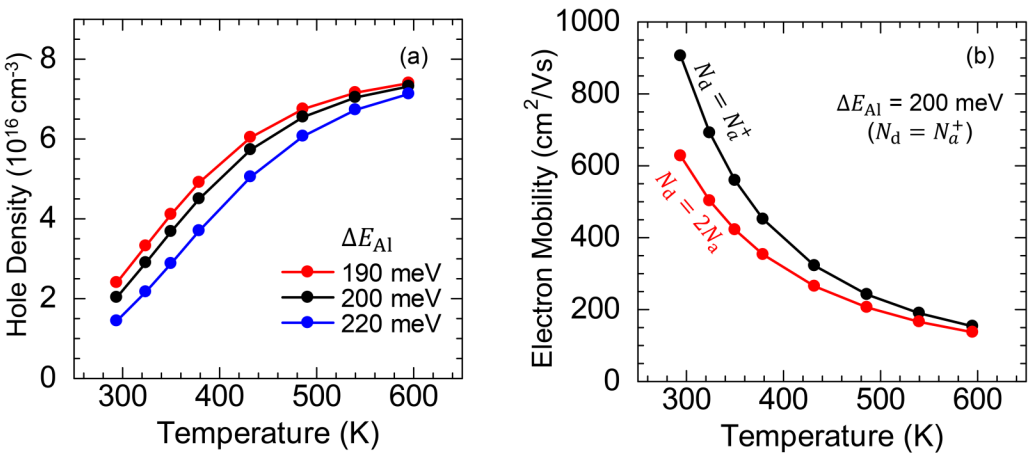

FIG. 4. (a) The temperature dependence of the hole density in the p-type base layer estimated assuming a single Al acceptor level, the ionization energy ΔE_{Al} of which ranges from 190 to 220 meV. (b) The temperature dependence of electron mobility in the p-type base layer estimated from the electron mobility in the n-type epilayers, whose doping concentrations were assumed as $N_d = N_a^+$ (black line) and $N_d = 2N_a$ (red line).

TABLE I. The calculation conditions (μ_n model) for electron mobility and parameters (ΔE_{Al}) for hole density in the base layer to deduce the minimum (n_{i_min}), middle (n_{i_mid}), and maximum (n_{i_max}) intrinsic carrier densities.

	μ_n model	ΔE_{Al} (meV)
n_{i_min}	$N_d = N_a^+$	220
n_{i_mid}	$N_d = N_a^+$	200
n_{i_max}	$N_d = 2N_a$	190

respectively. Despite the difficulty in estimating the actual hole density in the base layer due to the ambiguous ionization energy of the Al acceptor, the actual hole density in the base layer is considered to take a value between the minimum and maximum values presented in Fig. 4(a). Here, it should be mentioned that the effective densities of states of hole N_V was calculated taking account of the non-parabolic multiple valence bands when deducing the hole density based on semiconductor statistics, which is described in detail later.

As for the electron mobility μ_n, although the electron mobility in the n-type SiC epilayer has been carefully investigated in previous studies,[42–46] the electron mobility in the p-type epilayer has not been measured due to the difficulty of the measurement. Accordingly, in this work, the electron mobility in the p-type epilayer was inferred from the latest electron mobility model in the n-type epilayer.[46] Figure 4(b) shows the temperature dependence of electron mobility in the p-type epilayer estimated assuming an electron mobility in the p-type epilayer equivalent to that in (i) the n-type epilayer, the donor concentration of which equals the ionized acceptor concentration ($N_d = N_a^+$) and (ii) the n-type epilayer, with a donor concentration equal to the summation of the completely ionized acceptor and hole concentration ($N_d = 2N_a$), where the completely ionized acceptors and holes act as Coulomb-scattering sources of electron conduction. Here, the ionization ratio was estimated by adopting Al acceptor ionization energy of 200 meV in the case of (i) $N_d = N_a^+$. The electron mobility in the p-type epilayer could take a value between the electron mobility of $N_d = N_a^+$ and $N_d = 2N_a$.

Given the fact that the hole density and electron mobility ranges are estimated, the intrinsic carrier density range of SiC can be determined from Eq. (3) and Figs. 3(b), 4(a), and 4(b). Here, the effective base width of 3.4 μm, which is shorter than the actual physical base thickness of 3.7 μm due to the depletion region, is employed to accurately deduce the intrinsic carrier density. The maximum (n_{i_max}), middle (n_{i_mid}), and minimum (n_{i_min}) values are obtained by adopting the calculation conditions for the electron mobility and hole density shown in Table I. Figure 5 demonstrates the temperature dependence of intrinsic carrier density of SiC as obtained from the electrical characteristics, where the estimation error is presented in the inset, which was defined by $2(n_{i\_max} - n_{i\_min})/(n_{i_{max}} + n_{i\_min})$. It should be stressed that the estimation error becomes smaller with increasing temperature because the hole density and electron mobility ranges both do the same. The smaller estimation error of the intrinsic carrier density at higher temperatures, 43% at 294 K and 8% at 595 K, could be an advantage compared to the conventional

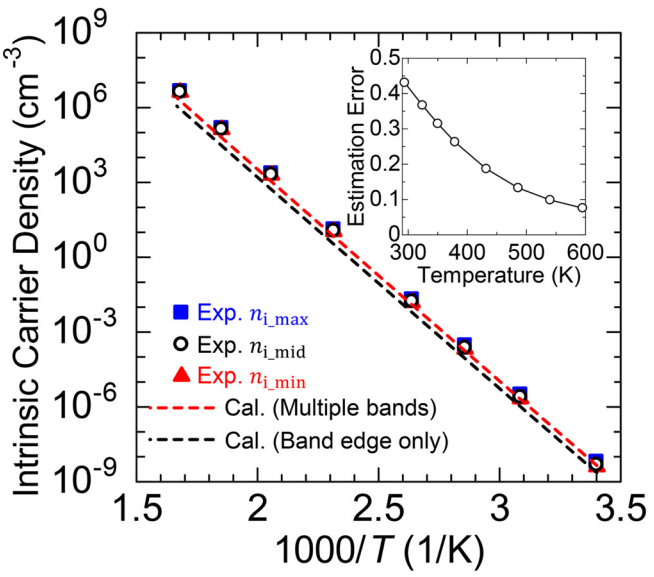

FIG. 5. The temperature dependence of the intrinsic carrier density. The blue square (n_{i_max}), open circle (n_{i_mid}), and red triangle (n_{i_min}) present the intrinsic carrier density deduced with the assumptions on the electron mobility and ionization energy of Al acceptor shown in Table I. The red and black dashed lines denote the values obtained using calculated effective densities of states and the constant bandgap of 3.26 eV. The inset shows the estimation error of the obtained intrinsic carrier density, which was defined by $2(n_{i\_max} - n_{i\_min})/(n_{i_{max}} + n_{i\_min})$.

method using the bandgap and effective densities of states, with a greater estimation error at elevated temperatures, as mentioned in Sec. I.

For comparison purpose, the conventional method is also employed to estimate the intrinsic carrier density using the following equation:

$$n_i^2 = N_C N_V \exp\left(-\frac{E_g}{kT}\right). \quad (4)$$

Here, N_C and N_V are the effective densities of states for the conduction band (electrons) and valence band (holes), respectively, and E_g denotes the SiC bandgap. The black and red dashed lines in Fig. 5 are the calculated intrinsic carrier densities, where the SiC bandgap is assumed to be a constant of 3.26 eV throughout the temperature range.[2,5,47] The difference in the black and red dashed lines is attributed to the effective densities of states. The black dashed line is obtained assuming that the electrons and holes exist only in the lowest conduction band and highest valence band, respectively, without considering the non-parabolicity of the band structure. In this case, the effective densities of states of electrons and holes become 1.8×10^{19} and 2.1×10^{19} cm^{-3} at 300 K, respectively.[2]

The red dashed line is calculated more precisely compared to the black dashed line by considering the complicated band structures. N_C is calculated taking account of the first and

second conduction band minimums at the M point, which is expressed as

$$N_C = 2M_C\left(\frac{2\pi m_{e1}kT}{h^2}\right)^{\frac{3}{2}} + 2M_C\left(\frac{2\pi m_{e2}kT}{h^2}\right)^{\frac{3}{2}}\exp\left(-\frac{E_{C2}-E_{C1}}{kT}\right). \quad (5)$$

Here, M_C, h, m_{e1}, m_{e2}, E_{C1}, and E_{C2} denote the number of the conduction band minimum, Plank constant, effective mass of electrons of the first band, effective mass of electrons of the second band, and the minimum energy of the first and second bands, respectively. The number of the conduction band is three ($M_C = 3$) and the effective masses were clarified as $m_{e1} = 0.390m_0$ and $m_{e2} = 0.445m_0$ for the first and second band, respectively, where m_0 is the electron mass.[7,48,49] The energy difference of the first and second conduction band minimum is $E_{C2} - E_{C1} = 0.12$ eV.[49,50]

The effective densities of states for holes N_V are also acquired by considering multiple and non-parabolic valence bands, where a $k \cdot p$ theory is adopted taking account of heavy hole, light hole, and crystal-field split-off hole bands.[51,52]

Figure 6 presents the temperature dependent effective densities of states for electrons and holes. The solid lines are values determined considering multiple bands and the dashed lines are obtained taking account of the parabolic first band only. The effective densities of states, particularly for holes, increase by considering multiple bands, which provides more accurate intrinsic carrier density.

As seen in Fig. 5, the intrinsic carrier density deduced by electrical measurement is in good agreement with the calculated value taking account of multiple bands (red dashed line), while the black dashed line is slightly lower than the experimental values. This suggests that the full band structures should be included to estimate the effective densities of states accurately. Here, the values of the intrinsic carrier density at room temperature (294 K) obtained in the present study are shown in Table II.

TABLE II. The values of the intrinsic carrier density at 294 K obtained in the present study. As a representative value of the experimentally obtained intrinsic carrier density, n_{i_mid} is exhibited. The calculated value taking account of multiple bands is also exhibited.

	From exp. (n_{i_mid})	From cal. (multiple bands)
Obtained n_i at 294 K	4.8×10^{-9} cm^{-3}	4.5×10^{-9} cm^{-3}

At the high temperature in Fig. 5, the values obtained by utilizing the BJT slightly exceed those calculated from the bandgap and effective densities of states (red dashed line). The slight discrepancy is attributable to the temperature dependence of the bandgap: the actual bandgap shrinks at high temperatures.

Figure 7 exhibits the temperature dependence of the bandgap, where the colored symbols denote the values obtained from Eq. (4) with adopting the experimentally induced intrinsic carrier densities, namely, n_{i_min}, n_{i_mid}, and n_{i_max}. The black dashed line presents the values deduced from the following empirical formula:[2]

$$E_g = E_{g0} - \frac{\alpha T^2}{T+\beta}. \quad (6)$$

Here, the empirical formula was derived from the temperature dependence of the SiC bandgap measured by optical measurements, where the E_g values exceeding 300 K are uncertain due to the indistinct absorption edge.[5] The empirical parameters α and β were determined as $\alpha = 8.2 \times 10^{-4}$ eV/K and $\beta = 1.8 \times 10^3$ K,

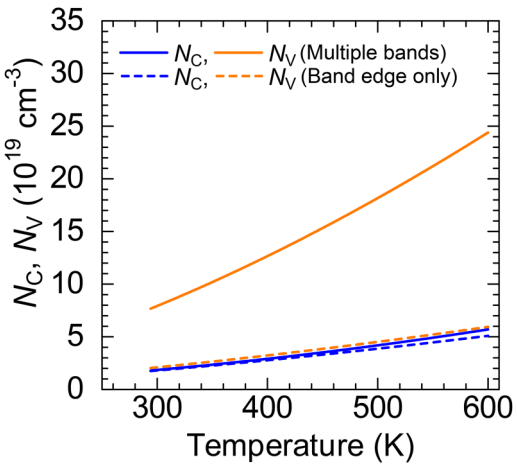

FIG. 6. The calculated effective densities of states for electrons (blue) and holes (orange). The solid lines indicate the calculated values taking account of multiple bands and the dashed lines denote the values considering the parabolic first band only.[2]

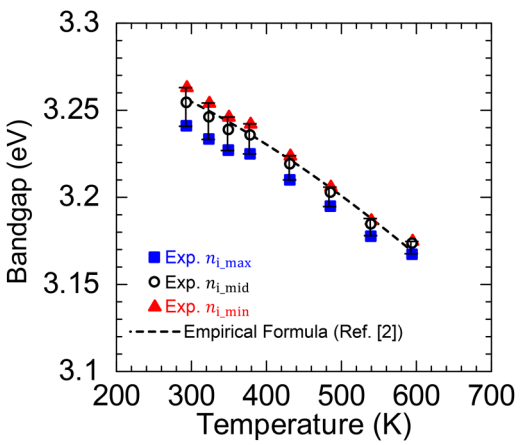

FIG. 7. The temperature dependence of the bandgap derived from the intrinsic carrier densities of n_{i_max} (blue square), n_{i_mid} (open circle), and n_{i_min} (red triangle) shown in Fig. 5. The black dashed line denotes the bandgap obtained from the empirical formula in the previous study.[2]

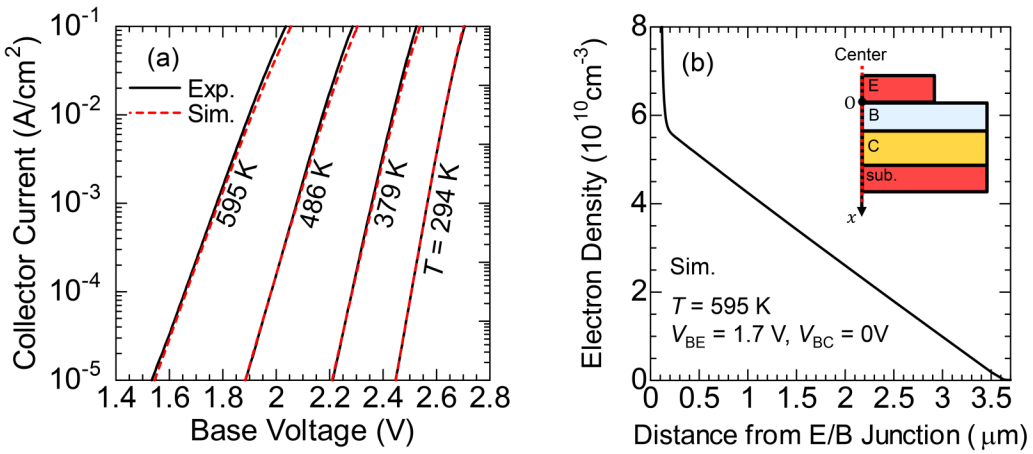

FIG. 8. (a) The experimental and simulated *I–V* characteristics of the fabricated BJTs, denoted by the black solid and red dashed lines, respectively, at temperatures from 294 to 595 K. (b) The simulated electron density distribution at the temperature of 595 K in the base layer with the applied base voltage of 1.7 V with retaining the base–collector voltage to zero. The distribution was obtained at the cross section of the center of the emitter finger, indicated by the red dashed line in the inset.

respectively, and the bandgap at 0 K of 3.29 eV was adopted ($E_{g0} = 3.29$ eV).[2]

The bandgap estimated from Eq. (4) agrees well with the values calculated from the empirical formula and the bandgap shrinkage at high temperatures is obviously observed. However, it is difficult to accurately determine the bandgap from the experimental intrinsic carrier density, given the ambiguous electron mobility in the p-type epilayer and ionization energy of the Al acceptor. Despite some remaining uncertainty in both the empirical formula and our experimental results, the present results suggest that the proposed method for measuring the intrinsic carrier density by utilizing a BJT could be useful in evaluating the bandgap energy. Since the estimation error of the bandgap in the proposed scheme becomes smaller with elevating temperature, the present method could be effective, particularly at high temperatures.

It is worth reaffirming that the proposed method is only applicable when the diffusion length of the electron in the base layer is longer than the base width and Eq. (2) is valid, as described in Sec. II. However, the carrier lifetime in the base layer was not measured due to the difficulty of the measurement. To prove the longer electron diffusion length than the base width at all measurement temperatures, the *I–V* characteristics of the BJT were simulated by TCAD while employing the intrinsic carrier density obtained in this study. Figure 8(a) shows the experimental and simulated *I–V* characteristics of the fabricated BJT, as denoted by the black solid and red dashed lines, respectively. As seen, the simulation reproduces well the experimental results at all temperatures. Since the TCAD simulation outputs the *I–V* characteristics by solving the current continuity and Poisson's equation without using the approximation of Eq. (2), the effective agreement between the simulated and experimental results indicates that the assumption of the longer electron diffusion length than the base width and the approximation of Eq. (2) is acceptable at all temperatures.

In fact, as presented in Fig. 8(b), the electron density linearly distributes in the base layer even at the temperature of 595 K, where the electron mobility and electron diffusion length are 153 $cm^2/V\,s$ and 8.8 μm, respectively, according to the mobility model of $N_d = N_a^+$ in Fig. 4(b). The recombination models and parameters for the simulation are summarized in Table III.

V. CONCLUSIONS

The intrinsic carrier density of SiC was obtained from the electrical characteristics of a SiC BJT. A suitable BJT structure for the present purpose was designed based on device simulations, and the designed BJT with a thick base layer and a large emitter finger width was fabricated. The intrinsic carrier density could be deduced by analyzing the collector current of the fabricated BJT

TABLE III. The carrier recombination models and parameters utilized for the device simulation. Shockley–Read–Hall (SRH), band to band, Auger, and surface recombination are incorporated. The parameters were chosen by referring the previous studies.

	Emitter	Base	Collector
Carrier lifetime for SRH recombination[28–31]	20 ns	100 ns	1 μs
Recombination coefficient for band to band recombination[53]		1.5×10^{-12} cm^3/s	
Recombination coefficient for Auger recombination[53]		5.0×10^{-31} cm^6/s (electron), 2.0×10^{-31} cm^6/s (hole)	
Surface recombination velocity[54]		3.0×10^7 cm/s	No surface region

assuming electron mobility in the p-type base epilayer and ionization energy of Al acceptor. The intrinsic carrier density obtained was in good agreement with a value calculated from the bandgap and effective densities of states taking multiple and non-parabolic SiC bands into account. The bandgap was also derived from the experimentally deduced intrinsic carrier density, which agreed well with the empirical formula for the SiC bandgap and clearly showed the shrinkage of the bandgap at high temperatures. The errors in evaluating the intrinsic carrier density and the bandgap caused by the estimation of the hole density and electron mobility in the base layer became smaller with elevating the temperature in the proposed method. Accordingly, the proposed method, which is also applicable to other semiconductor materials, could be useful to obtain the intrinsic carrier density and bandgap at high temperatures.

ACKNOWLEDGMENTS

This work was supported by JSPS KAKENHI (Grant No. JP21K14203).

AUTHOR DECLARATIONS

Conflict of Interest

The authors have no conflicts to disclose.

Author Contributions

Satoshi Asada: Conceptualization (lead); Data curation (lead); Formal analysis (lead); Funding acquisition (lead); Investigation (lead); Methodology (lead); Writing – original draft (lead). **Koichi Murata:** Data curation (equal); Formal analysis (equal); Writing – review & editing (equal). **Hajime Tanaka:** Data curation (equal); Formal analysis (equal); Writing – review & editing (equal). **Hidekazu Tsuchida:** Resources (lead); Supervision (lead); Writing – review & editing (lead).

DATA AVAILABILITY

The data that support the findings of this study are available from the corresponding author upon reasonable request.

REFERENCES

[1]M. A. Green, J. Appl. Phys. **67**, 2944 (1990).
[2]T. Kimoto and J. A. Cooper, *Fundamentals of Silicon Carbide Technology* (John Wiley & Sons Singapore Pte. Ltd., 2014).
[3]M. D. Sturge, Phys. Rev. **127**, 768 (1962).
[4]W. J. Turner, W. E. Reese, and G. D. Pettit, Phys. Rev. **136**, A1467 (1964).
[5]W. J. Choyke, Mater. Res. Bull. **4**, S141 (1969).
[6]R. N. Dexter, H. J. Zeiger, and B. Lax, Phys. Rev. **104**, 637 (1956)..
[7]W. M. Chen, N. T. Son, E. Janzén, D. M. Hofmann, and B. K. Meyer, Phys. Status Solidi **162**, 79 (1997)..
[8]F. J. Morin and J. P. Maita, Phys. Rev. **96**, 28 (1954).
[9]M. Bhatnagar and B. J. Baliga, IEEE Trans. Electron Devices **40**, 645 (1993).
[10]M. Ruff, H. Mitlehner, and R. Helbig, IEEE Trans. Electron Devices **41**, 1040 (1994).
[11]A. Itoh, T. Kimoto, and H. Matsunami, IEEE Electron Device Lett. **17**, 139 (1996).
[12]D. T. Morisette and J. A. Cooper, IEEE Trans. Electron Devices **49**, 1657 (2002).
[13]H. Niwa, J. Suda, and T. Kimoto, Appl. Phys. Express **5**, 064001 (2012).
[14]S. M. Sze and K. K. Ng, *Physics of Semiconductor Devices*, 3rd ed. (Wiley Interscience, 2007).
[15]K. Wada, T. Kimoto, K. Nishikawa, and H. Matsunami, J. Cryst. Growth **291**, 370 (2006).
[16]S. Asada, J. Suda, and T. Kimoto, IEEE Trans. Electron Devices **66**, 4870 (2019).
[17]S. Asada, J. Suda, and T. Kimoto, IEEE Trans. Electron Devices **67**, 1699 (2020).
[18]G. Y. Chung, C. C. Tin, J. R. Williams, K. McDonald, R. K. Chanana, R. A. Weller, S. T. Pantelides, L. C. Feldman, O. W. Holland, M. K. Das, and J. W. Palmour, IEEE Electron Device Lett. **22**, 176 (2001).
[19]L. Lanni, B. Malm, M. Ostling, and C.-M. Zetterling, IEEE Electron Device Lett. **34**, 1091 (2013).
[20]S.-H. Ryu, A. K. Agarwal, R. S. Singh, and J. W. Palmour, IEEE Electron Device Lett. **22**, 124 (2001).
[21]K. Tachiki, K. Mikami, K. Ito, M. Kaneko, and T. Kimoto, Appl. Phys. Express **15**, 071001 (2022).
[22]J. A. Cooper, M. R. Melloch, R. Singh, A. Agarwal, and J. W. Palmour, IEEE Trans. Electron Devices **49**, 658 (2002).
[23]H. Miyake, T. Kimoto, and J. Suda, IEEE Electron Device Lett. **32**, 841 (2011).
[24]Q. Zhang, A. Agarwal, A. Burk, B. Geil, and C. Scozzie, Solid. State Electron. **52**, 1008 (2008).
[25]H. Miyake, T. Kimoto, and J. Suda, IEEE Electron Device Lett. **32**, 285 (2011).
[26]H.-S. Lee, M. Domeij, C.-M. Zetterling, M. Östling, F. Allerstam, and E. Ö. Sveinbjornsson, Appl. Phys. Lett. **92**, 082113 (2008).
[27]K. Nonaka, A. Horiuchi, Y. Negoro, K. Iwanaga, S. Yokoyama, H. Hashimoto, M. Sato, Y. Maeyama, M. Shimizu, and H. Iwakuro, Mater. Sci. Forum **615–617**, 821 (2009).
[28]P. A. Ivanov, M. E. Levinshtein, A. K. Agarwal, S. Krishnaswami, and J. W. Palmour, IEEE Trans. Electron Devices **53**, 1245 (2006).
[29]B. Buono, R. Ghandi, M. Domeij, B. Malm, C.-M. Zetterling, and M. Ostling, IEEE Trans. Electron Devices **57**, 704 (2010).
[30]S. Ichikawa, K. Kawahara, J. Suda, and T. Kimoto, Appl. Phys. Express **5**, 101301 (2012).
[31]T. Okuda, T. Kimoto, and J. Suda, Appl. Phys. Express **6**, 121301 (2013).
[32]S. Asada, T. Kimoto, and J. Suda, IEEE Trans. Electron Devices **64**, 2086 (2017).
[33]S. Asada, J. Suda, and T. Kimoto, Mater. Sci. Forum **924**, 629 (2018).
[34]B. Buono, R. Ghandi, M. Domeij, B. G. Malm, C.-M. Zetterling, and M. Ostling, IEEE Trans. Electron Devices **57**, 2664 (2010).
[35]S. Asada, J. Suda, and T. Kimoto, IEEE Trans. Electron Devices **65**, 2771 (2018).
[36]S. Asada, T. Okuda, T. Kimoto, and J. Suda, Jpn. J. Appl. Phys. **54**, 070309 (2015).
[37]A. Koizumi, J. Suda, and T. Kimoto, J. Appl. Phys. **106**, 013716 (2009).
[38]S. Asada, T. Okuda, T. Kimoto, and J. Suda, Appl. Phys. Express **9**, 041301 (2016).
[39]S. Contreras, L. Konczewicz, R. Arvinte, H. Peyre, T. Chassagne, M. Zielinski, and S. Juillaguet, Phys. Status Solidi **214**, 1600679 (2017).
[40]A. Parisini and R. Nipoti, J. Appl. Phys. **114**, 243703 (2013).
[41]G. Pensl, F. Schmid, F. Ciobanu, M. Laube, S. A. Reshanov, N. Schulze, K. Semmelroth, H. Nagasawa, A. Schöner, and G. Wagner, Mater. Sci. Forum **433–436**, 365 (2003).
[42]J. Pernot, W. Zawadzki, S. Contreras, J. L. Robert, E. Neyret, and L. Di Cioccio, J. Appl. Phys. **90**, 1869 (2001).
[43]J. Pernot, S. Contreras, J. Camassel, J. L. Robert, W. Zawadzki, E. Neyret, and L. Di Cioccio, Appl. Phys. Lett. **77**, 4359 (2000).
[44]J. Pernot, S. Contreras, and J. Camassel, J. Appl. Phys. **98**, 023706 (2005).
[45]H. Iwata and K. M. Itoh, J. Appl. Phys. **89**, 6228 (2001).
[46]R. Ishikawa, M. Hara, H. Tanaka, M. Kaneko, and T. Kimoto, Appl. Phys. Express **14**, 061005 (2021).

[47]W. J. Choyke and R. P. Devaty, *Optical Properties of SiC: 1997-200, in Silicon Carbide-Recent Major Advances* (Springer, 2004).
[48]D. Volm, B. K. Meyer, D. M. Hofmann, W. M. Chen, N. T. Son, C. Persson, U. Lindefelt, O. Kordina, E. Sörman, A. O. Konstantinov, B. Monemar, and E. Janzén, Phys. Rev. B **53**, 15409 (1996).
[49]C. Persson and U. Lindefelt, J. Appl. Phys. **82**, 5496 (1997).
[50]S. Lyu and W. R. L. Lambrecht, Phys. Rev. B **102**, 79904 (2020).
[51]T. Hatakeyama, K. Fukuda, and H. Okumura, IEEE Trans. Electron Devices **60**, 613 (2013).
[52]H. Tanaka, S. Asada, T. Kimoto, and J. Suda, J. Appl. Phys. **123**, 245704 (2018).
[53]A. Galeckas, J. Linnros, V. Grivickas, U. Lindefelt, and C. Hallin, Appl. Phys. Lett. **71**, 3269 (1997).
[54]S. Asada, J. Suda, and T. Kimoto, IEEE Trans. Electron Devices **65**, 4786 (2018).